JACS
JOURNAL OF THE AMERICAN CHEMICAL SOCIETY
pubs.acs.org/JACS
Article

Liquid Phase Edge Epitaxy of Transition-Metal Dichalcogenide Monolayers

Sabir Hussain, Rui Zhou, You Li, Ziyue Qian, Zunaira Urooj, Misbah Younas, Zhaoyang Zhao, Qinghua Zhang, Wenlong Dong, Yueyang Wu, Xiaokai Zhu, Kangkang Wang, Yuansha Chen, Luqi Liu, and Liming Xie*

Cite This: J. Am. Chem. Soc. 2023, 145, 11348−11355
Read Online
ACCESS | Metrics & More | Article Recommendations | Supporting Information

ABSTRACT: Precise monolayer epitaxy is important for two-dimensional (2D) semiconductors toward future electronics. Here, we report a new self-limited epitaxy approach, liquid phase edge epitaxy (LPEE), for precise-monolayer epitaxy of transition-metal dichalcogenides. In this method, the liquid solution contacts 2D grains only at the edges, which confines the epitaxy only at the grain edges and then precise monolayer epitaxy can be achieved. High-temperature in situ imaging of the epitaxy progress directly supports this edge-contact epitaxy mechanism. Typical transition-metal dichalcogenide monolayers (MX_2, M = Mo, W, and Re; X = S or Se) have been obtained by LPEE with a proper choice of molten alkali halide solvents (AL, A = Li, Na, K, and Cs; L = Cl, Br, or I). Furthermore, alloying and magnetic-element doping have also been realized by taking advantage of the liquid phase epitaxy approach. This LPEE method provides a precise and highly versatile approach for 2D monolayer epitaxy and can revolutionize the growth of 2D materials toward electronic applications.

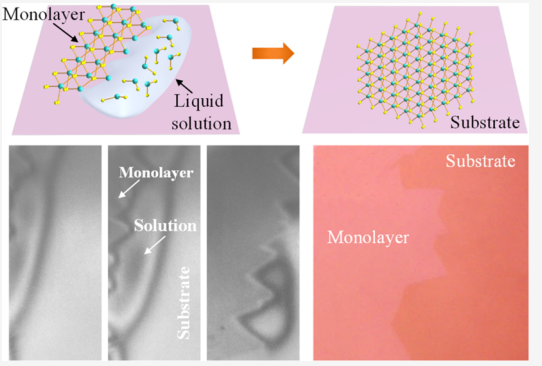

INTRODUCTION

Two-dimensional (2D) materials have garnered tremendous research interest due to their atomic thickness yet no dangling bond on the surfaces.[1,2] Semiconducting 2D materials, such as transition-metal dichalcogenides,[3,4] can scale the physical size of transistors down to 1 nm, which makes them promising candidate channel materials for future electronics.[5,6] Precise monolayer growth of 2D materials is of great importance to the ultra-short channel transistors; however, it is of great challenge.[7−13] An effective approach for thickness control is via self-limited growth,[14] in which the growth is confined at the interface and then the thickness can be controlled by the growth mechanism.[15,16] A successful example is the growth of graphene on copper, where the copper catalysis limits the graphene growth only on the copper surface, and hence only graphene monolayer can be grown but not the thicker layers.[17] Interface reactions have also been utilized for the self-limited growth of 2D materials. For example, nitrogen species were dissolved in melting the Au film and reacted with gaseous borazine for all monolayer growth of BN.[18] Mo spices were dissolved in glass and reacted with sulfur vapor for the growth of MoS_2 monolayers.[19,20] Atomic layer deposition (ALD) has also been used in MoS_2 growth, but the film quality is low.[21]

Here, we have developed a new versatile self-limited growth method for high-quality 2D monolayers: liquid phase edge epitaxy (LPEE). In this method, the transition-metal dichalcogenide monolayer is grown from a molten solution on a substrate (Figure 1a). The solution contacts the 2D grains only at the grain edges, which limits the epitaxy only at the edges and a uniform monolayer has been obtained. In situ high-temperature optical imaging has been carried out and showed a direct evidence of the epitaxial process along the monolayer edges. The quality of as-prepared monolayers has been examined by atomic-resolution scanning transmission electron microscopy (STEM), showing high-quality single crystalline domains. Furthermore, LPEE has been successfully tested for different transition-metal dichalcogenides (MX_2, M = Mo, W, and Re; X = S or Se) with different molten alkali halide solvents (AL, A = Li, Na, K, and Cs; L = Cl, Br, or I). Benefitting from the liquid phase epitaxy, various 2D monolayer alloys ($MoS_{2(1-x)}Se_{2x}$, $Mo_{(1-x)}WxS_2$, $WS_{2(1-x)}Se_{2x}$, and $W_{(1-x)}Re_xS_2$) and 2D monolayers doped with magnetic elements (Cr/MoS_2, Fe/MoS_2, Co/MoS_2, Ni/MoS_2, $Cr/MoSe_2$, $Fe/MoSe_2$, $Co/MoSe_2$, $Ni/MoSe_2$, and Ni/WS_2) have been obtained.

Received: March 8, 2023
Published: May 12, 2023

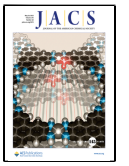

Downloaded via INST OF PHYSICS on December 3, 2023 at 14:48:09 (UTC).
See https://pubs.acs.org/sharingguidelines for options on how to legitimately share published articles.

© 2023 American Chemical Society

https://doi.org/10.1021/jacs.3c02471
J. Am. Chem. Soc. 2023, 145, 11348−11355

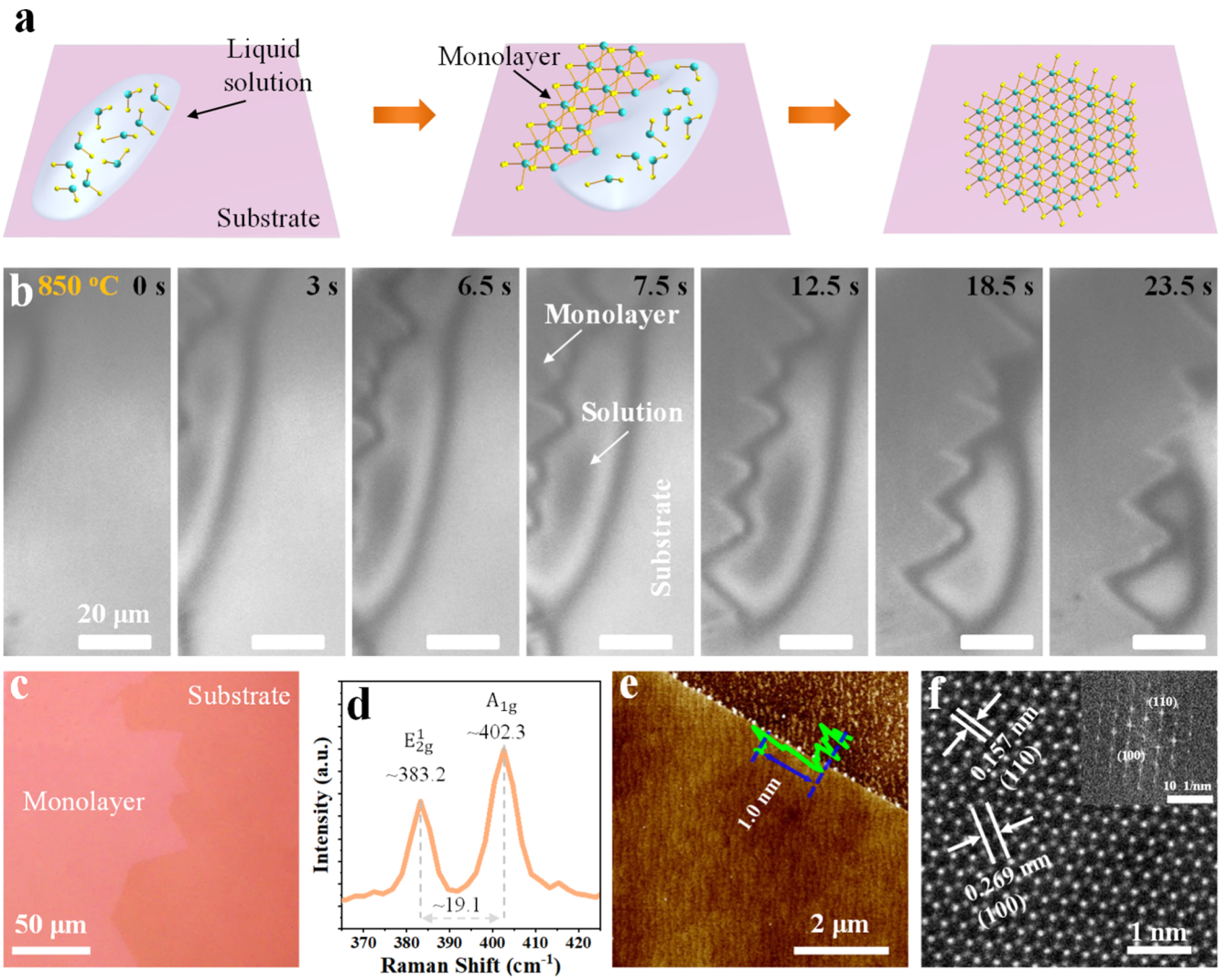

Figure 1. LPEE of MoS_2 monolayers from its CsCl solution. (a) Illustration of the LPEE process. (b) In situ imaging of LPEE of MoS_2 monolayers from the CsCl solution at 850 °C. (c–f) Optical microscopy image, Raman spectrum, AFM image, and STEM image (with the inset of the FFT) of as-prepared MoS_2 monolayers, respectively.

RESULTS AND DISCUSSION

In a typical experiment of MoS_2 monolayer epitaxy from its CsCl solution at 850 °C, MoS_2 in CsCl solution was condensed on a sapphire substrate for LPEE (Methods and Figure S1). A home-built high-temperature optical microscope[22] was equipped into the CVD furnace to record the in situ growth process. The in situ optical imaging clearly showed that the MoS_2 flake was growing (with a rate of 1–2 μm/s) as the liquid droplet was moving (Figure 1b). The liquid droplet contacted the MoS_2 flake only at the flake edges but not over the flake, which physically prevented nucleation and growth on the MoS_2 flake and inhibited few-layers growth. The liquid droplet size decreased as the flake epitaxy occurred, suggesting that the epitaxy driving force (i.e., the supersaturation) was from the evaporation of the solvent.

The MoS_2 thin film showed a homogeneous optical contrast, indicating a uniform thickness (Figure 1c). Raman spectroscopic characterization and AFM imaging confirmed the monolayer thickness of the MoS_2 film (A_{1g} and E^1_{2g} difference of 19.1 cm^{-1}, Figure 1d; and AFM height of 1.0 nm, Figure 1e).[23,24] The homogeneous color contrast in AFM imaging shows an ultra-clean basal plane of the MoS_2 flake and is free of few-layer domains and particle contaminations.[25] Atomic-resolution STEM imaging (Figure 1f) showed a perfect hexagonal lattice of the MoS_2 film with clearly resolved Mo atoms and S atoms. The atom line spacing of 0.269 nm, matches well with the (100) plane spacing of MoS_2. In the fast Fourier transform (FFT) of the STEM image (the inset in Figure 1f), a single set of hexagonal spots was observed, indicating the single crystalline nature for the flake.[26,27] The experimental parameters including the growth time and the growth temperature affect the growth result significantly (Figures S2–S4). As the growth time increases, the coverage and size of MoS_2 monolayers increase (Figures 2 and S2,S3). Full coverage of the MoS_2 monolayer on the sapphire substrate was obtained for a 3.5 h growth.[28,29] Benefitting from the edge epitaxy mechanism of LPEE, no bilayer or few-layer was observed (Figure 2h).

Furthermore, TEM, STEM, Raman mappings, and electrical measurements on the as-grown MoS_2 monolayers indicate a high crystal quality of the monolayers (Figures S5–S9). Raman spectra show no degradation after 15 days for TMDC monolayers, which suggests a high ambient stability of the as-grown monolayers in air (Figure S17). To evaluate the

https://doi.org/10.1021/jacs.3c02471
J. Am. Chem. Soc. 2023, 145, 11348–11355

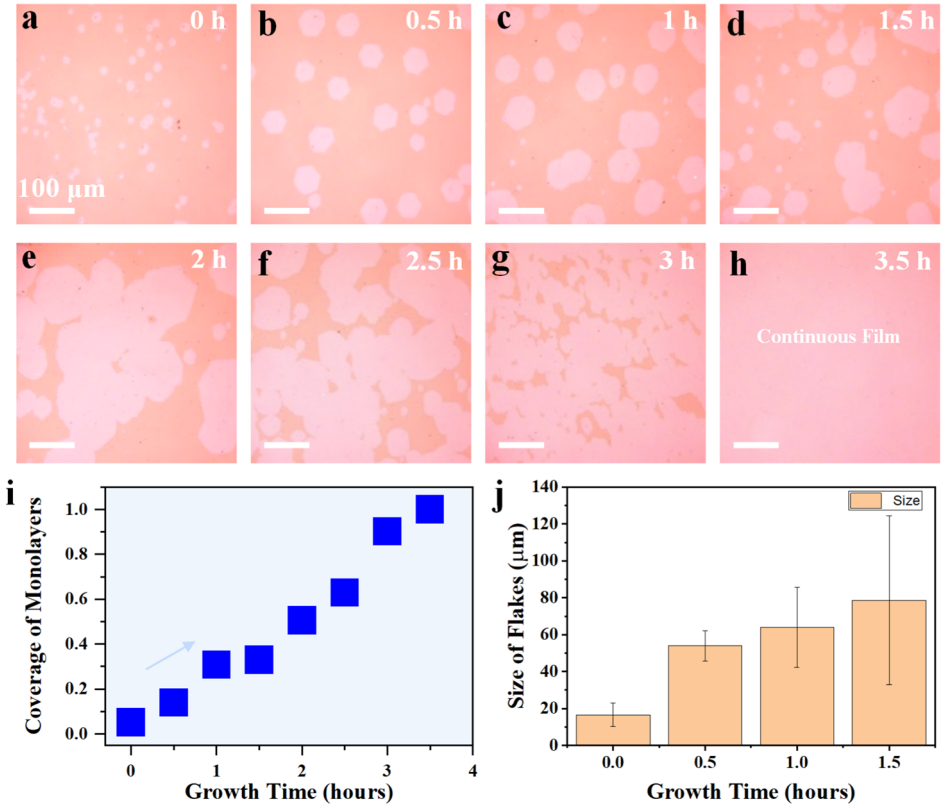

Figure 2. LPEE of MoS_2 monolayers to a full coverage. (a–h) Optical images of as-prepared MoS_2 monolayers on sapphire substrates with different epitaxy times. The solvent was molten CsCl and the growth temperature was 850 °C. (i,j) Monolayer coverage and flake size of MoS_2 monolayers at different growth times.

thermal stability of our grown monolayers, temperature-dependent Raman test under nitrogen protection was conducted, showing that the monolayers can be stable up to 350 °C (Figures S18 and S19).

The monolayer growth behavior of LPEE was further tested for different transition-metal dichalcogenides with different solvents. With proper molten alkali halide solvents, many transition-metal dichalcogenide monolayers (MX_2, M = Mo, W, and Re; X = S or Se) were obtained (Figure 3). Optical images showed homogeneous contrast for the as-prepared MX_2 flakes. The MX_2 flake size ranged from a few micrometers to more than a hundred micrometers. AFM and Raman characterization were also done to confirm the monolayer thickness of the flakes (Figures S10–S15).

The monolayer yields for different MX_2 with different molten solvents are plotted in Figure 4a. Not all MX_2-AL combinations showed uniform-monolayer epitaxy. For example, the epitaxy of transition-metal dichalcogenides from the LiCl solutions yielded thick flakes (Figure S16). Excluding LiCl, a trend can be seen for other solvents, which is that the monolayer growth is more preferred for solvents with higher surface tensions (Figure 4b).[30,37] This can be understood by the dewetting condition for liquid droplets on MX_2,[16,31]

$$\gamma_{l-g} > \frac{\gamma_{2D-g} - \gamma_{2D-l}}{\cos\theta}$$

Where $\gamma_{l\text{-}g}$ is the surface tension of the solution, $\gamma_{2D\text{-}g}$ is the surface tension of the 2D-material, $\gamma_{2D\text{-}l}$ is the surface tension between the 2D material and the solution, and θ is the contact angle of the droplet on the 2D material flake.[32]

A higher liquid surface tension is more favored for dewetting the solution from the MX_2 flake which can make the edge-contact more possible (Figure 4b left).[33,34] Meanwhile, a lower liquid surface tension prefers wetting of the MX_2 flake, which can result in few-layer nucleation and growth (Figure 4b right).[35] The exception for LiCl may be due to the small ion radius of Li^+[36] and a strong affinity of LiCl to MX_2, which results in a low value of $\gamma_{2D\text{-}l}$ and wetting of the MX_2 flakes.

A great advantage of liquid phase edge epitaxy is the easy alloying and doping of the monolayers. Based on the successful epitaxy of MX_2 monolayers with the selected solvents, various monolayer alloys, such as $MoS_{2(1-x)}Se_{2x}$, $Mo_{(1-x)}WxS_2$, $WS_{2(1-x)}Se_{2x}$, and $W_{(1-x)}Re_xS_2$, have been obtained (Figures 5 and S20–S23). Taking $MoS_{2(1-x)}Se_{2x}$ as an example, AFM measurement confirmed the monolayer thickness of the alloys (0.6–1.0 nm). Raman characterization showed that the compositions were continuously tuned by changing the mass ratios of the alloying materials (Figure S20). Photoluminescence (PL) emission measurements revealed continuous band gap tuning in the near-infrared regions (Figure 5b). The energy-dispersive X-ray spectroscopy (EDS) mapping showed homogeneous elemental distributions of the Mo, S, and Se elements all over the flake (Figure 5c). Atomic resolution STEM imaging showed different intensity sites (Figure 5d), which also confirmed the successful alloying of MoS_2 and $MoSe_2$.[38,39]

Doping atomically thin semiconductors with magnetic elements is of great interest toward spin electronics. Using the advantages of the LPEE method, Cr/Fe/Co/Ni-doped MX_2 semiconducting monolayers have been obtained by adding $CrCl_2$, $FeCl_2$, $CoCl_2$, or $NiCl_2$ into the liquid solutions

https://doi.org/10.1021/jacs.3c02471
J. Am. Chem. Soc. 2023, 145, 11348–11355

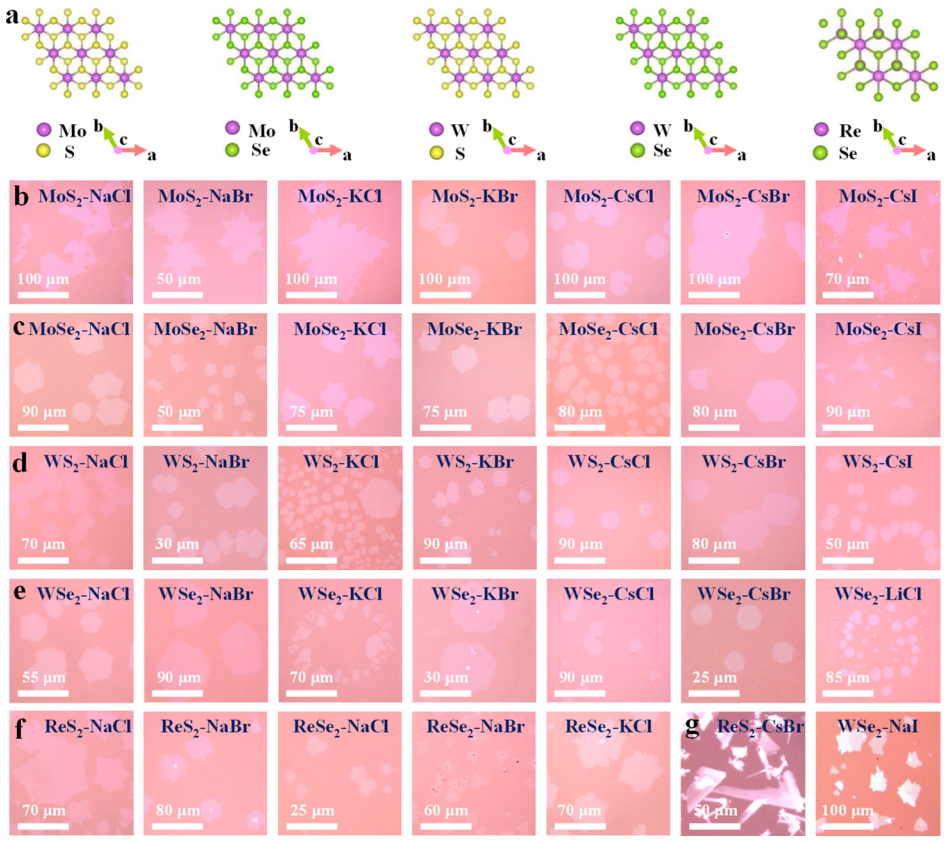

Figure 3. LPEE of various transition-metal dichalcogenide monolayers with selected molten alkali halide solvents. (a) Structures of MoS_2, $MoSe_2$, WS_2, WSe_2, and ReX_2 (X = S, Se). (b–f) Optical images for the epitaxial monolayers: MoS_2, $MoSe_2$, WS_2, WSe_2, and ReX_2, respectively. (g) Optical images of epitaxy of MX_2 with non-uniform thickness.

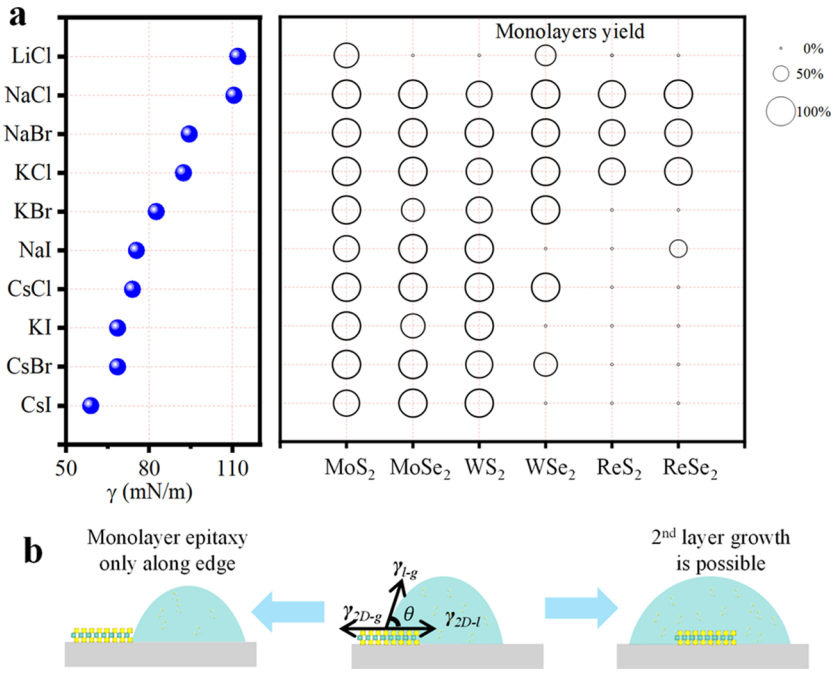

Figure 4. Correlation between the monolayer yield and the surface tension of the molten solvents used in LPEE. (a) The plot of surface tensions of molten alkali metal halides (data for T = 850 °C)[37] and plot of the monolayer yield for different pairs of MX_2-alkali metal halide. (b) Illustration of the dewetting case (left) and the wetting case (right) which depends on the surface tensions.

(Figures S24–S27). For Co-doped $MoSe_2$ as an example (Figure 6), AFM imaging showed a film thickness of 0.9 nm, indicating the monolayer nature (Figure S26). PL emission showed a redshift from 791 to 821 nm, along with quenching and broadening of the emission peaks after Co doping (Figure 6b). This is due to the doping-induced trion emission and

https://doi.org/10.1021/jacs.3c02471
J. Am. Chem. Soc. 2023, 145, 11348–11355

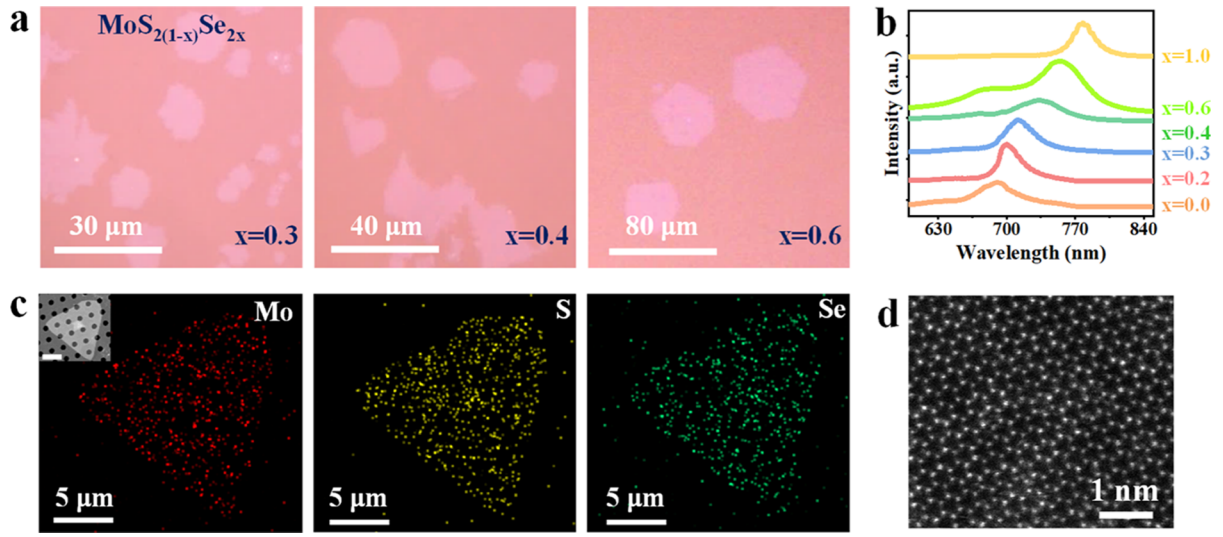

Figure 5. LPEE of monolayer alloys. (a) Optical images, (b) PL spectra, (c) element mapping, and (d) atomic-resolution STEM image of LPEE grown $MoS_{2(1-x)}Se_{2x}$ monolayers.

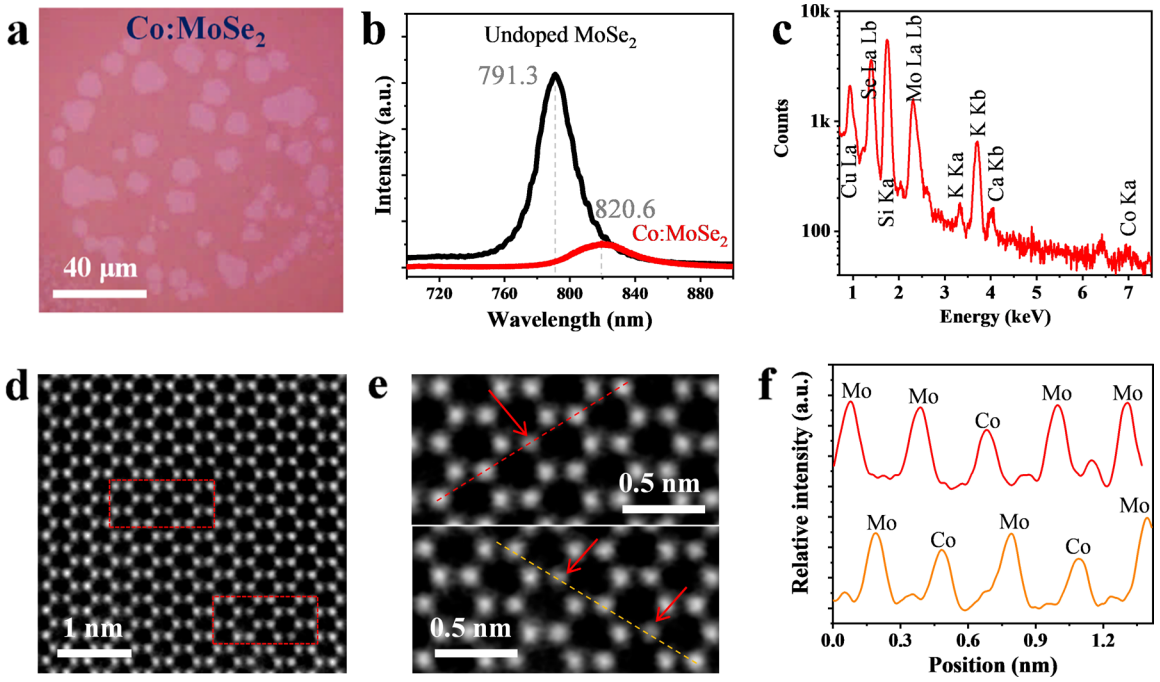

Figure 6. LPEE of Co-doped $MoSe_2$ monolayers. (a) Optical image, (b) PL spectrum, and (c) EDS spectrum of Co-doped $MoSe_2$ monolayers. (d) STEM image of a Co-doped $MoSe_2$ monolayer, (e) zoom-in images (the red arrows indicate the atoms with dimmer intensities), and (f) the intensity section analysis along the lines in panel e.

band gap modulation, which is similar to the reported observation in Re/V-doped MX_2 monolayers.[40−42] EDS measurement showed a Co Ka peak at 6.9 keV with an atomic percentage of 0.27% for the Co-doped $MoSe_2$ monolayer. Atomic-resolution STEM imaging (Figure 6d−f) also revealed Co doping sites with dimmer intensities. Other magnetic element doped monolayers have been obtained and some with significant $M-H$ loops at low temperatures, such as $Fe/MoSe_2$ (Figure S25).[43,44]

■ CONCLUSIONS

Overall, we have developed an edge-contact LPEE for the growth of high-quality monolayers, monolayer alloys, and magnetic-element doped monolayers of transition-metal dichalcogenides. In situ optical imaging directly supports the edge epitaxy mechanism. EDS mapping and atomic-resolution STEM imaging have confirmed the high quality of the monolayers, the successful alloying, and the doping. Cross-experiments on multiple MX_2 and molten solvent combinations have revealed that surface tension plays an important role in the LPEE. This LPEE method provides a precise and highly versatile approach for 2D monolayer epitaxy with tunable compositions/doping and can revolutionize the growth of 2D materials toward electronic applications.

https://doi.org/10.1021/jacs.3c02471
J. Am. Chem. Soc. 2023, 145, 11348−11355

EXPERIMENTAL SECTION

Growth Recipe. LPEE was done in a single temperature zoon chemical vapor deposition (CVD) furnace under atmospheric pressure. Transition-metal dichalcogenide precursor source (Alfa Aesar, purity 99.999%) and alkali metal salt source (Alfa Aesar, purity 99.998%) were loaded in a quartz boat with a ratio of 1:20. Sapphire substrates with a c-plane (0001) were placed directly above the boat (see Supplementary Figure 1). Before heating, the system was vacuum pumped for 10 min and flushed with high-purity 50 sccm Ar gas to expel air. The furnace temperature was ramped to the growth temperature (800−900 °C) within 30 min and maintained the growth temperature for 0−3.5 h. 10 sccm Ar gas was utilized as the carrier gas during the growth. After growth, the furnace was naturally cooled down with flowing Ar gas.

In Situ Imaging Furnace. The system consists of a CVD furnace with an optical access hole, a high-temperature resistant objective, a light-emitting diode (LED) monochrome light source (488 nm), a CCD, and other minor parts.

Characterizations. Optical images were captured on a Olympus BX51 optical microscope, and Raman/PL characterization was done on a home-built Raman/PL spectroscopy with 532 nm excitation. The laser power was kept below 0.5 mW μm^{-2} to avoid sample damage. The contact mode of Asylum Research MFP-3D Infinity AFM (Oxford Instruments) was used to explore the thickness mappings of 2D materials. X-ray photoelectron spectroscopy (XPS) spectra were acquired using an ESCALAB250Xi (ThermoFisher Scientific, UK). Without specification, all measurements were done at room temperature.

HAADF-STEM Sample Preparation and Characterization. The monolayer samples were transferred onto TEM grids by a wet polymethyl methacrylate (PMMA) transfer method. A layer of PMMA of about 1 μm thick was first spin-coated on the substrate with deposited samples and then baked at 80 °C for 15 min. The substrate was then immersed in distilled water for 15 min to separate the substrate. The PMMA/TMD film was fished by a TEM grid and baked at 120 °C for 10 min, and then dropped into acetone overnight to dissolve the PMMA coating layers. The STEM of MoS_2 was conducted by a double Cs-corrected JEOL JEM-ARM200CF operated at 200 kV with a CEOS Cs corrector (CEOS GmbH, Heidelberg, Germany) in the Institute of Physics, Chinese Academy of Sciences. The HAADF-STEM images were recorded with a collection semi-angle of 90−370 mrad. For the STEM images and EDX of $MoS_{2(1-x)}Se_{2x}$, Themis Z was operated at 300 kV in Scientific Compass, Beijing. The probe current was 50 pA. The HAADF-STEM image was recorded at a convergence semi-angle of a 25 mrad and an inner angle of 41 mrad. For the STEM images and EDX of Co/$MoSe_2$, a JEM-ARM200F with a CEOS corrector with a cold-FEG was operated at 200 kV in Migelab, Beijing. The HAADF-STEM image was recorded at a convergence angle of 20 mrad and a detected angle of 68 mrad.

ASSOCIATED CONTENT

Supporting Information

The Supporting Information is available free of charge at https://pubs.acs.org/doi/10.1021/jacs.3c02471.

Growth and characterizations of as-synthesized MX2, alloy, and magnetically doped monolayers along with magnetic properties (PDF)

AUTHOR INFORMATION

Corresponding Author

Liming Xie − *CAS Key Laboratory of Standardization and Measurement for Nanotechnology, National Center for Nanoscience and Technology, Beijing 100190, China; University of Chinese Academy of Sciences, Beijing 100049, China;* orcid.org/0000-0001-8190-8325; Email: xielm@nanoctr.cn

Authors

Sabir Hussain − *CAS Key Laboratory of Standardization and Measurement for Nanotechnology, National Center for Nanoscience and Technology, Beijing 100190, China;* orcid.org/0000-0002-9259-5376

Rui Zhou − *CAS Key Laboratory of Standardization and Measurement for Nanotechnology, National Center for Nanoscience and Technology, Beijing 100190, China; University of Chinese Academy of Sciences, Beijing 100049, China*

You Li − *CAS Key Laboratory of Standardization and Measurement for Nanotechnology, National Center for Nanoscience and Technology, Beijing 100190, China; University of Chinese Academy of Sciences, Beijing 100049, China*

Ziyue Qian − *CAS Key Laboratory of Standardization and Measurement for Nanotechnology, National Center for Nanoscience and Technology, Beijing 100190, China; University of Chinese Academy of Sciences, Beijing 100049, China*

Zunaira Urooj − *CAS Key Laboratory of Standardization and Measurement for Nanotechnology, National Center for Nanoscience and Technology, Beijing 100190, China; University of Chinese Academy of Sciences, Beijing 100049, China*

Misbah Younas − *CAS Key Laboratory of Standardization and Measurement for Nanotechnology, National Center for Nanoscience and Technology, Beijing 100190, China; University of Chinese Academy of Sciences, Beijing 100049, China*

Zhaoyang Zhao − *CAS Key Laboratory of Standardization and Measurement for Nanotechnology, National Center for Nanoscience and Technology, Beijing 100190, China; University of Chinese Academy of Sciences, Beijing 100049, China*

Qinghua Zhang − *Beijing National Laboratory for Condensed Matter Physics, Institute of Physics, Chinese Academy of Sciences, Beijing 100190, China*

Wenlong Dong − *CAS Key Laboratory of Standardization and Measurement for Nanotechnology, National Center for Nanoscience and Technology, Beijing 100190, China; University of Chinese Academy of Sciences, Beijing 100049, China*

Yueyang Wu − *Key Laboratory of Organic Optoelectronics and Molecular Engineering of the Ministry of Education, Department of Chemistry, Tsinghua University, Beijing 100084, China*

Xiaokai Zhu − *CAS Key Laboratory of Standardization and Measurement for Nanotechnology, National Center for Nanoscience and Technology, Beijing 100190, China; University of Chinese Academy of Sciences, Beijing 100049, China*

Kangkang Wang − *CAS Key Laboratory of Standardization and Measurement for Nanotechnology, National Center for Nanoscience and Technology, Beijing 100190, China; University of Chinese Academy of Sciences, Beijing 100049, China*

Yuansha Chen − *Beijing National Laboratory for Condensed Matter Physics, Institute of Physics, Chinese Academy of Sciences, Beijing 100190, China*

Luqi Liu − *CAS Key Laboratory of Standardization and Measurement for Nanotechnology, National Center for Nanoscience and Technology, Beijing 100190, China;*

University of Chinese Academy of Sciences, Beijing 100049, China; orcid.org/0000-0002-5752-1638

Complete contact information is available at: https://pubs.acs.org/10.1021/jacs.3c02471

Author Contributions

H.S. and R.Z. contributed equally to this work. L.X. conceived the project. H.S. carried out the growth, Raman/PL/AFM/device characterizations. R.Z. performed the in situ experiments, alloy growth, and STEM sample preparation. Y.L. and Z.Q. assisted with the alloy growth. Z.Z. developed a home-built in-situ CVD system. W.D. and L.L. assisted with the AFM characterization. Y.W. assisted with the Hall bar device characterizations. All authors participated in the data analysis and contributed to the manuscript writing.

Notes

The authors declare no competing financial interest.

■ ACKNOWLEDGMENTS

L.X. acknowledges support from the Strategic Priority Research Program of CAS (XDB30000000) and the National Key R&D Program of China (2020YFB2205901). The authors thanks to the Division of Nanotechnology Development and the Nanofab Lab of the National Center for Nanoscience and Technology (NCNST) for the characterization and device fabrications.

■ REFERENCES

(1) Chhowalla, M.; Shin, H. S.; Eda, G.; Li, L. J.; Loh, K. P.; Zhang, H. The chemistry of two-dimensional layered transition metal dichalcogenide nanosheets. *Nat. Chem.* **2013**, *5*, 263−275.

(2) Ajayan, P.; Kim, P.; Banerjee, K. Two-dimensional van der Waals materials. *Phys. Today* **2016**, *69*, 38−44.

(3) Zhou, J.; Lin, J.; Huang, X.; Zhou, Y.; Chen, Y.; Xia, J.; Wang, H.; Xie, Y.; Yu, H.; Lei, J.; Wu, D.; Liu, F.; Fu, Q.; Zeng, Q.; Hsu, C.; Yang, C.; Lu, L.; Yu, T.; Shen, Z.; Lin, H.; Yakobson, B. I.; Liu, Q.; Suenaga, K.; Liu, G.; et al. A library of atomically thin metal chalcogenides. *Nature* **2018**, *556*, 355−359.

(4) Kim, T.; Dhakal, K.; Park, E.; Noh, G.; Chai, H.; Kim, Y.; Oh, S.; Kang, M.; Park, J.; Kim, J.; Kim, S.; Jeong, H.; Bang, S.; Kwak, J.; Kim, J.; Kang, K. Gas-phase alkali metal-assisted MOCVD growth of 2D transition metal dichalcogenides for large-scale precise nucleation control. *Small* **2022**, *18*, 2106368.

(5) Desai, S. B.; Madhvapathy, S. R.; Sachid, A. B.; Llinas, J. P.; Wang, Q.; Ahn, G. H.; Pitner, G.; Kim, M. J.; Bokor, J.; Hu, C.; Wong, H. S. P.; Javey, A. MoS_2 transistors with 1-nanometer gate length. *Science* **2016**, *354*, 99−102.

(6) Wu, F.; Tian, H.; Shen, Y.; Hou, Z.; Ren, J.; Gou, G.; Sun, Y.; Yang, Y.; Ren, T. L. Vertical MoS_2 transistors with sub-1-nm gate lengths. *Nature* **2022**, *603*, 259−264.

(7) Xu, X.; Das, G.; He, X.; Hedhili, M. N.; Fabrizio, E. D.; Zhang, X.; Alshareef, H. N. High-performance monolayer MoS_2 films at the wafer scale by two-step growth. *Adv. Funct. Mater.* **2019**, *29*, 1901070.

(8) Liao, M.; Wei, Z.; Du, L.; Wang, Q.; Tang, J.; Yu, H.; Wu, F.; Zhao, J.; Xu, X.; Han, B.; Liu, K.; Gao, P.; Polcar, T.; Sun, Z.; Shi, D.; Yang, R.; Zhang, G. Precise control of the interlayer twist angle in large scale MoS_2 homostructures. *Nat. Commun.* **2020**, *11*, 2153.

(9) Liu, F.; Li, P.; An, H.; Peng, P.; Mclean, B.; Ding, F. Achievements and Challenges of Graphene Chemical Vapor Deposition Growth. *Adv. Mater.* **2022**, *32*, 2203191.

(10) Xu, X.; Das, G.; He, X.; Hedhili, M. N.; Fabrizio, E. D.; Zhang, X.; Alshareef, H. N. High-performance monolayer MoS_2 films at the wafer scale by two-step growth. *Adv. Funct. Mater.* **2019**, *29*, 1901070.

(11) Chen, C.; Feng, Z.; Feng, Y.; Yue, Y.; Qin, C.; Zhang, D.; Feng, W. Large-scale synthesis of a uniform film of bilayer MoS_2 on graphene for 2D heterostructure phototransistors. *ACS Appl. Mater. Interfaces* **2016**, *8*, 19004−19011.

(12) Gao, Q.; Zhang, Z.; Xu, X.; Song, J.; Li, X.; Wu, Y. Scalable high performance radio frequency electronics based on large domain bilayer MoS_2. *Nat. Commun.* **2018**, *9*, 4778.

(13) Fu, D.; Zhao, X.; Zhang, Y.; Li, L.; Xu, H.; Jang, A.; Yoon, S.; Song, P.; Poh, S.; Ren, T.; Ding, Z.; Fu, W.; Shin, T.; Shin, H. S.; Pantelides, S. T.; Zhou, W.; Loh, K. P. Molecular beam epitaxy of highly crystalline monolayer molybdenum disulfide on hexagonal boron nitride. *J. Am. Chem. Soc.* **2017**, *139*, 9392−9400.

(14) Zhang, J.; Lin, L.; Jia, K.; Sun, L.; Peng, H.; Liu, Z. Controlled growth of single-crystal graphene films. *Adv. Mater.* **2020**, *32*, 1903266.

(15) Wan, X.; Chen, K.; Xie, W.; Wen, J.; Chen, H.; Xu, J. B. Quantitative analysis of scattering mechanisms in highly crystalline CVD MoS_2 through a self-limited growth strategy by interface engineering. *Small* **2016**, *12*, 438−445.

(16) Sirat, M. S.; Ismail, E.; Ramlan, A. H.; Fauzi, F. B.; Yaacob, I. I.; Mohamed, M. A.; Azam, M. A.; Ani, M. H. Influence of surface energy and elastic strain energy on the graphene growth in chemical vapor deposition. *Mater. Today: Proc.* **2019**, *7*, 776−783.

(17) Li, X.; Cai, W.; An, J.; Kim, S.; Nah, J.; Yang, D.; Piner, R.; Velamakanni, A.; Jung, I.; Tutuc, E.; Banerjee, S. K.; Colombo, L.; Ruoff, R. S. Large-area synthesis of high-quality and uniform graphene films on copper foils. *Science* **2009**, *324*, 1312−1314.

(18) Lee, J. S.; Choi, S. H.; Yun, S. J.; Kim, Y. I.; Boandoh, S.; Park, J.; Shin, B. G.; Ko, H.; Lee, S. H.; Kim, Y. M.; Lee, Y. H.; Kim, K. K.; Kim, S. M. Wafer-scale single-crystal hexagonal boron nitride film via self-collimated grain formation. *Science* **2018**, *362*, 817−821.

(19) Lu, Y.; Chen, T.; Ryu, G. H.; Huang, H.; Sheng, Y.; Chang, R. J.; Warner, J. H. Self-limiting growth of high-quality 2D monolayer MoS_2 by direct sulfurization using precursor-soluble substrates for advanced field-effect transistors and photodetectors. *ACS Appl. Nano Mater.* **2018**, *2*, 369−378.

(20) Cai, Z. Y.; Lai, Y. J.; Zhao, S. L.; Zhang, R. J.; Tan, J. Y.; Feng, S. M.; Zou, J.; Tang, L.; Lin, J.; Liu, B.; Cheng, H. Dissolution-precipitation growth of uniform and clean two dimensional transition metal dichalcogenides. *Natl. Sci. Rev.* **2021**, *8*, nwaa115.

(21) Tan, L. K.; Liu, B.; Teng, J. H.; Guo, S.; Low, H. Y.; Loh, K. P. Atomic layer deposition of a MoS_2 film. *Nanoscale* **2014**, *6*, 10584−10588.

(22) Xie, L.; Zhi, Z.; Zhao, Z. A high-temperature material growth system with in situ optical microscopic imaging and in situ microscopic Raman spectroscopy measurement. *Chinese Patent* **2022**, *4*, 202110662304.

(23) Liu, L.; Wu, J.; Wu, L.; Ye, M.; Liu, X.; Wang, Q.; Hou, S.; Lu, P.; Sun, L.; Zheng, J.; Xing, L.; Gu, L.; Jiang, X.; Xie, L.; Jiao, L. Phase-selective synthesis of 1T′ MoS_2 monolayers and heterophase bilayers. *Nat. Mater.* **2018**, *17*, 1108−1114.

(24) Voiry, D.; Fullon, R.; Yang, J.; de Carvalho Castro e Silva, C.; Kappera, R.; Bozkurt, I.; Kaplan, D.; Lagos, M. J.; Batson, P. E.; Gupta, G.; Mohite, A. D.; Dong, L.; Er, D.; Shenoy, V. B.; Asefa, T.; Chhowalla, M. The role of electronic coupling between substrate and 2D MoS_2 nanosheets in electrocatalytic production of hydrogen. *Nat. Mater.* **2016**, *15*, 1003−1009.

(25) Hussain, S.; Xu, R.; Xu, K.; Lei, L.; Meng, L.; Zheng, Z.; Xing, S.; Guo, J.; Dong, H.; Liaqat, A.; Iqbal, M. A.; Li, Y.; Sugawara, Y.; Pang, F.; Ji, W.; Xie, L.; Cheng, Z. Strain-induced hierarchical ripples in MoS_2 layers investigated by atomic force microscopy. *Appl. Phys. Lett.* **2020**, *117*, 153102.

(26) Li, Y.; Wang, H.; Xie, L.; Liang, Y.; Hong, G.; Dai, H. MoS_2 nanoparticles grown on graphene: an advanced catalyst for the hydrogen evolution reaction. *J. Am. Chem. Soc.* **2011**, *133*, 7296−7299.

(27) Zhu, D.; Shu, H.; Jiang, F.; Lv, D.; Asokan, V.; Omar, O.; Yuan, J.; Zhang, Z.; Jin, C. Capture the growth kinetics of CVD growth of two-dimensional MoS_2. *npj 2D Mater. Appl* **2017**, *1*, 8.

(28) Yang, P.; Zou, X.; Zhang, Z.; Hong, M.; Shi, J. P.; Chen, S.; Shu, J.; Zhao, L.; Jiang, S.; Zhou, X.; Huan, Y.; Xie, C.; Gao, P.; Chen,

Q.; Zhang, Q.; Liu, Z.; Zhang, Y. Batch production of 6-inch uniform monolayer molybdenum disulfide catalyzed by sodium in glass. *Nat. Commun.* **2018**, *9*, 979.
(29) Han, W.; Zheng, X.; Yang, K.; Tsang, C.; Zheng, F.; Wong, L.; Lai, K. H.; Yang, T.; Wei, Q.; Li, M.; Io, W.; Guo, F.; Cai, Y.; Wang, N.; Hao, J.; Lau, S. P.; Lee, C.; Ly, T. H.; Yang, M.; Zhao, J. Phase-controllable large-area two-dimensional In_2Se_3 and ferroelectric heterophase junction. *Nat. Nanotechnol.* **2023**, *18*, 55−63.
(30) van Zeggeren, F.; Benson, G. C. Calculation of the surface energies of alkali halide crystals. *J. Chem. Phys.* **1957**, *26*, 1077−1082.
(31) Chaudhury, M. K.; Whitesides, G. M. How to make water run uphill. *Science* **1992**, *256*, 1539−1541.
(32) Zhang, X.; Cai, X.; Jin, K.; Jiang, Z.; Yuan, H.; Jia, Y.; Wang, Y.; Cao, L.; Zhang, X. Determining the surface tension of two-dimensional nanosheets by a low-rate advancing contact angle measurement. *Langmuir* **2019**, *35*, 8308−8315.
(33) Jiang, D.; Wang, X.; Chen, R.; Sun, J.; Kang, H.; Ji, D.; Liu, Y.; Wei, D. Self-expanding molten salt-driven growth of patterned transition-metal dichalcogenide crystals. *J. Am. Chem. Soc.* **2022**, *144*, 8746−8755.
(34) Li, S.; Lin, Y.; Zhao, W.; Wu, J.; Wang, Z.; Hu, Z.; Shen, Y.; Tang, D.; Wang, J.; Zhang, Q.; Zhu, H.; Chu, L.; Zhao, W.; Liu, C.; Sun, Z.; Taniguchi, T.; Osada, M.; Chen, W.; Xu, Q.; Wee, A. T. S.; Suenaga, K.; Ding, F.; Eda, G. Vapour-liquid-solid growth of monolayer MoS_2 nanoribbons. *Nat. Mater.* **2018**, *17*, 535−542.
(35) Wang, H.; Orejon, D.; Song, D.; Zhang, X.; McHale, G.; Takamatsu, H.; Takata, Y.; Sefiane, K. Non-wetting of condensation-induced droplets on smooth monolayer suspended graphene with contact angle approaching 180 degrees. *Commun. Mater.* **2022**, *3*, 75.
(36) David, L.; Bhandavat, R.; Singh, G. MoS_2/Graphene composite paper for sodium-Ion battery electrodes. *ACS Nano* **2014**, *8*, 1759−1770.
(37) Goodisman, J. Surface tensions of molten salt mixtures. *J. Colloid Interface Sci.* **1980**, *73*, 115−123.
(38) Feng, Q.; Mao, N.; Wu, J.; Xu, H.; Wang, C.; Zhang, J.; Xie, L. Growth of $MoS_{2(1-x)}Se_{2x}$ (x = 0.41-1.00) monolayer alloys with controlled morphology by physical vapor deposition. *ACS Nano* **2015**, *9*, 7450−7455.
(39) Feng, Q.; Zhu, Y.; Hong, J.; Zhang, M.; Duan, W.; Mao, N.; Wu, J.; Xu, H.; Dong, F.; Lin, F.; Jin, C.; Wang, C.; Zhang, J.; Xie, L. Growth of large-area 2D $MoS_{2(1-x)}Se_{2x}$ semiconductor alloys. *Adv.Mater.* **2014**, *26*, 2648−2653.
(40) Kozhakhmetov, A.; Schuler, B.; Tan, A. M. Z.; Cochrane, K. A.; Nasr, J. R.; El-Sherif, H.; Bansal, A.; Vera, A.; Bojan, V.; Redwing, J. M.; Bassim, N.; Das, S.; Hennig, R. G.; Weber-Bargioni, A.; Robinson, J. A. Scalable substitutional Re-doping and its impact on the optical and electronic properties of tungsten diselenide. *Adv. Mater.* **2020**, *32*, 2005159.
(41) Kozhakhmetov, A.; Stolz, S.; Tan, A. M. Z.; Pendurthi, R.; Bachu, S.; Turker, F.; Alem, N.; Kachian, J.; Das, S.; Hennig, R. G.; Groning, O.; Schuler, B.; Robinson, J. A. Controllable p-type doping of 2D WSe_2 via vanadium substitution. *Adv. Funct. Mater.* **2021**, *31*, 2105252.
(42) Li, S.; Hong, J.; Gao, B.; Lin, Y.; Lim, H.; Lu, X.; Wu, J.; Liu, S.; Tateyama, Y.; Sakuma, Y.; Tsukagoshi, K.; Suenaga, K.; Taniguchi, T. Tunable doping of rhenium and vanadium into transition metal dichalcogenides for two-dimensional electronics. *Adv. Sci.* **2021**, *8*, 2004438.
(43) Tian, Y.; Zhu, Z.; Ge, Z.; Sun, A.; Zhang, Q.; Huang, S.; Li, H.; Meng, J. Electronic and magnetic properties of 3d transition metal doped $MoSe_2$ monolayer. *Physica E* **2020**, *116*, 113745.
(44) Shen, D.; Zhao, B.; Zhang, Z.; Zhang, H.; Yang, X.; Huang, Z.; Li, B.; Song, R.; Jin, Y.; Wu, R.; Li, B.; Li, J.; Duan, X. Synthesis of group VIII magnetic transition-metal-doped monolayer $MoSe_2$. *ACS Nano* **2022**, *16*, 10623−10631.

https://doi.org/10.1021/jacs.3c02471
J. Am. Chem. Soc. 2023, 145, 11348−11355